Numerical investigation on the collapse of a bubble cluster near a solid wall

Lingxin Zhang, Jing Zhang, and Jian Deng*
Department of Mechanics, Zhejiang University, Hangzhou 310027, People's Republic of China

(Received 18 January 2019; published 24 April 2019)

This paper studies numerically the collapse of a cluster of cavitation bubbles (as a primitive model for a bubble cloud) near a solid wall. The homogeneous two-phase mixture model is used, with the liquid-vapor interface resolved by volume of fluid method. The liquid is treated as compressible, allowing the propagation of pressure waves at the speeds determined by a state equation. This cluster consists of 27 identical bubbles, evenly distributed in a cubic region, with various bubble-wall and bubble-bubble distances considered. Our simulations suggest that the bubble-wall distance plays a more significant role. The maximum impulsive pressure of 41 MPa is achieved when the cluster is very close to the wall. The inward progress of collapse is observed by examining the evolutions of bubble shapes and flow fields, with two distinctly different sequences of collapse identified between the small and large bubble-wall distances. At a large bubble distance, the centermost bubble is the last to collapse, while at a small bubble distance, it is the central bubble nearest to the wall which collapses lastly. This difference can also explain the more intensive impulsive pressure for the smaller bubble-wall distances. The proposed numerical approach is of special interest because it can resolve the details of bubble-bubble and bubble-wall interactions, which are significant to the study of the collapse of a cavitation cloud, and its potential damage to hydraulic systems.

DOI: 10.1103/PhysRevE.99.043108

I. INTRODUCTION

The collapse of cavitation bubble is a strongly nonlinear problem, which has been studied for decades owing to its negative effects on hydraulic facilities, which should be avoided or at least controlled [1]. For example, the strong microjets and the high pressure impulses induced around the collapsing bubbles may severely damage solid walls by removing material from the surface, leading to serious erosion in valves and associated hydraulic equipment [2–4]. It is well known that the ability of collapsing cavitation bubbles to focus and concentrate energy is at the root of cavitation damage, sonochemistry, or sonoluminescence [5–7]. This unique ability to focus energy can also be put to remarkably constructive use. Cavitation bubbles are now used in a remarkable range of surgical and medical procedures, for example, to emulsify tissue (most commonly in cataract surgery or in lithotripsy procedures for the reduction of kidney and gall stones) or to manipulate the DNA in individual cells [8]. By creating cavitation bubbles noninvasively thereby depositing and focusing energy nonintrusively, one can generate minute incisions or target cancer cells [9,10].

It was recognized a century ago in Lord Rayleigh's work [11] that the pressure in the liquid outside a collapsing bubble can be predicted to reach upward of 100 bar in a few tens to hundreds of nanoseconds. Rayleigh proposed a transport equation of spherically symmetrical cavitation bubble, assuming that the surrounding liquid is incompressible and inviscid, and the surface tension is negligible [11]. Plesset [12], Noltingk and Neppiras [13], and Poritsky [14] modified this equation to include the effects of viscosity, surface tension, and incident sound waves. Considering the compressibility of the liquid, the Keller-Miksis equation was proposed to model the finite-amplitude bubble oscillations [15], which has been used in most modern studies [16]. The theoretical models of bubbles have been continuously developed. More recently, different variations of Rayleigh-Plesset–type equations were proposed to describe the finite-amplitude oscillation of a bubble in a liquid-filled cavity confined by an elastic solid owing to the possible medical applications to soft tissues [17–20].

In contrast to the spherically symmetric configurations in most theoretical models, it is more practical to consider the cavitation bubble collapsing near a wall. As early as 1944, it was realized by Kornfeld and Suvorov [21] that microjetting can be a dominant mechanism in the collapse of a cavitation bubble in liquid. It is well known now that a liquid jet can be formed in a collapsing bubble due to inhomogeneities in the pressure field when the collapsing cavity is close to a solid wall, as predicted by Plesset and Chapman [22] through solving numerically the potential flow, and verified experimentally by Lauterborn and Bolle [2]. Then, a series of experiments were performed by the same research group to accurately measure the jetting flows by time-resolved particle velocimetry (PIV) [23,24].

It was followed by the experiments concerning different aspects of this problem, such as the collapse of a pair of bubbles [25–28], the bubble-sphere interactions [29], the bubble collapsing between two perpendicular rigid walls [30], the collapse of large bubbles in a highly overpressured environment [31], the cavitation bubbles in liquid mercury [32], and a wide variety of nonspherical bubbles induced by new laser techniques [33]. In those experiments, the bubbles were induced by ultrasonics, laser pulses, electric sparks, or even

*Corresponding author: zjudengjian@zju.edu.cn

by mechanical impacts. Technically, it is possible to generate multiple bubbles, or a bubble cluster, as reported by Cui *et al.* [34], up to four bubbles were generated at the crossed joints of thin copper alloy wires with energy from the discharge of a capacitor. However, it is extremely challenging to get uniform and evenly distributed bubbles due to the difficult setup in traditional techniques, though some efforts have been made [35].

Alternatively, Bremond *et al.* produced well-controlled hemispherical surface bubbles by using a hydrophobic surface patterned with microcavities [36]. It was observed that during the cluster collapse the individual bubbles collapsed aspherically and developed a jetting flow toward the cluster's center. By examining the evolution of bubbles, they found that the pressure wave traveled at the speed of sound in the water. Similarly, arrays of transient cavitation bubbles could also be obtained by shaping a pulsed laser beam with digital hologram and focusing it into a thin gap of liquid [37]. However, we note that both experiments were based on two-dimensional configurations, or the bubble cluster distributed on a surface. The real three-dimensional experiments have rarely been carried out.

As a fast algorithm, with inviscid and incompressible assumptions, the boundary element method (BEM) has been developed and applied to study the bubble-wall and bubble-bubble interactions [38,39]. For the bubble near a flat plate in the presence of a shear flow, they found that the bubble elongated during its growth with the increasing ratio between the shear flow velocity and bubble collapse velocity. For a cluster of bubbles, they reported that the collapse proceeded from the outer bubble shells toward the inside, indicating a cloud period of oscillation much larger than that of individual bubbles. We note that both studies indicate the profound nonspherical deformations caused by the confinement from either the wall or the surrounding bubbles.

With the development of computing resources, direct simulations of the Navier-Stokes equations become possible for the bubble dynamics studies, with different treatments for the liquid-vapor interfaces, such as the volume of fluid (VOF) [40] and level set methods [41,42]. Nevertheless, the direct simulations of bubble collapse are still challenging due to the fact that most existing numerical codes assume that the liquids are incompressible, which makes the propagation of pressure waves impossible to be correctly captured. Therefore, the detailed bubble-scale dynamics of a cluster remain poorly quantified. Recently, compressible-fluid multiphase-flow equations were solved to investigate a cluster of gas bubbles, including all mesh-revolved bubble-bubble interactions and the nonspherical dynamics of each bubble within the cluster, with a 50-bubble cluster considered adjacent to a rigid wall [43]. Although the dynamics of gas bubbles is different from that of cavitation bubbles, it is instructive to the dynamics of cavitation bubble clusters.

In this paper, we present numerical simulations of a cluster of cavitation bubbles, consisting of 27 individuals. A numerical model is proposed, which considers the compressibility of the liquid and the detailed bubble-bubble and bubble-wall interactions. Our primary aim is to evaluate the impulsive pressure induced by the pressure wave emitted by the bubble collapse, and investigate the asymmetric collapses of the bubbles.

II. NUMERICAL METHODOLOGY

A. Numerical model

We consider the fluid containing bubbles as a homogeneous two-phase mixture, which is simulated by the direct numerical simulation (DNS) method. A transport equation for the liquid volume fraction is adopted to capture the interface between two phases. The viscosity, surface tension, and compressibility of the fluid are also taken into account. The governing equations can be expressed as follows:

$$\frac{d\rho}{dt} + \rho\nabla\cdot\mathbf{U} = 0, \tag{1}$$

$$\rho\frac{\partial\mathbf{U}}{\partial t} + \rho\mathbf{U}\cdot\nabla\mathbf{U} = \rho\mathbf{g} - \nabla p + 2\nabla\cdot(\mu\mathbf{D}) - \frac{2}{3}\nabla(\mu\nabla\cdot\mathbf{U}) + \sigma\kappa\mathbf{N}, \tag{2}$$

$$\frac{d\alpha}{dt} = \frac{\partial\alpha}{\partial t} + \mathbf{U}\cdot\nabla\alpha = 0, \tag{3}$$

where $\mathbf{U}$ and p are the velocity and pressure, respectively. $\mathbf{D}$ is the strain rate tensor ($\mathbf{D} = [\nabla\mathbf{U} + (\nabla\mathbf{U})^T]/2$), k is the surface curvature, σ is the surface tension coefficient, $\mathbf{N}$ is the unit normal vector of the interface, and α is the volume fraction of the liquid. ρ and μ are the density and viscosity of the mixture, respectively, which are obtained by the weighting of each volume fraction:

$$\rho = \alpha\rho_1 + (1-\alpha)\rho_2, \tag{4}$$

$$\mu = \alpha\mu_1 + (1-\alpha)\mu_2, \tag{5}$$

where subscripts "1" and "2" denote the liquid phase (water) and the gas phase (vapor), respectively. When the mixture is considered as a compressible medium, the equation of state (EOS) of each phase should be supplied. However, the thermal physics of vapor bubble is still not fully understood due to the contribution from latent heat. As a simplification, the Rayleigh-Plesset equation [11] assumes that the pressure in vapor bubbles can be kept constant when modeling the motion of spherical bubbles. Following this assumption, we set the pressure and density within the vapors to be constant values. The EOS for the liquid phase [44] can be expressed as

$$\rho_1 = \rho_{10} + \frac{1}{c_1^2}p, \tag{6}$$

where ρ_{10} is the density constant, c_1 is the speed of sound in liquid. Here, we set $\rho_{10} = 998\ \mathrm{kg/m^3}$ and $c_1 = 1500\ \mathrm{m/s}$.

The pressure-based method has been widely used in water flow computations. Typically, a pressure equation can be derived from the continuity equation. However, as the compressibility of liquid phase has been involved in the modeling, the dependency of density and pressure should be supplied in the derivation. Previously, our group has developed a robust SIMPLE-like pressure-based algorithm for the computations of compressible two-phase flows [45]. This algorithm is also employed in this study.

In our simulations, the space discretizations are second-order upwind for the convection terms and central differences for the Laplacian terms, respectively. The time discretization

is first-order implicit Euler. The preconditioned conjugate gradient (PCG) method is used to treat the pressure equation and the preconditioned biconjugate gradient (PBiCG) method is used for the velocity equations.

B. Validation

To validate our numerical model, we first study a single cavitation bubble. The computational domain is a cuboid with dimensions of 48 mm × 48 mm × 30 mm. A bubble with a radius of 2.02 mm is placed 2.29 mm above the central point of the bottom of the computational domain. After carefully carrying out self-consistency tests, we find that the grid with a cell number 6,480,000 (180 × 180 × 200) and an initial maximum time step size $dt = 1e^{-7}$ s are sufficient to ensure satisfactory independence of the results with respect to both mesh and time discretizations. The grid is nonuniform Cartesian grid, which is refined around the bubble with 41 cells distributed along the bubble diameter. The time step size is adjustable during the simulations to meet the requirement of local courant number Co = 0.35. The bottom of the computational domain is a solid wall, and the other boundaries are with fixed constant pressure and zero gradients of the velocities normal to the boundary surfaces.

Dimensionless bubble-wall distance, pressure, and time are defined, respectively, as

$$\gamma = \frac{L}{R_0}, \quad p^* = \frac{p}{p_\infty - p_0}, \quad t^* = \frac{t}{t_c}, \tag{7}$$

where L is the distance between the bubble and the solid wall, R_0 is the initial radius of the bubble, p_∞ is the far-field pressure, p_0 is the initial pressure (vapor pressure) inside the bubble, and t_c is the time span of bubble collapse obtained from the solution to an unbounded spherical bubble [11], with the formula

$$t_c = 0.915 R_0 \sqrt{\frac{\rho_l}{p_\infty - p_0}}, \tag{8}$$

where ρ_l is the liquid density, which is approximately equal to ρ_{l0} shown in (6) due to the very weak compressibility of the liquid. We also define a dimensionless time span of collapse as $\kappa = t_s/t_c$, where t_s is the time span of bubble collapse obtained from our numerical simulations.

In Fig. 1(a), we show the outlines of the bubble during collapse, where $\gamma = 1.13$. During the first phase, from 0 to 123 μs, the confinement of the solid wall causes the bubble to elongate slightly along the axis perpendicular to the wall. It is followed by surface perturbations in the upper portion of the bubble, resulting in a more rapid collapse of the upper portion, and eventually forming a jetting flow toward the wall. The present simulations are consistent with the previous experiment, as shown in Fig. 1(b).

To further validate our numerical model, we carry out a series of simulations by varying the distance γ. The initial radius of the bubble is set to $R_0 = 1$ mm to make a direct comparison with the formula derived by Rattray, which was also used in Ref. [47]. This comparison in the time spans of collapse with various dimensionless distances is shown in Fig. 2, with a good agreement made between the analytic solution and the present numerical simulations. Here, we

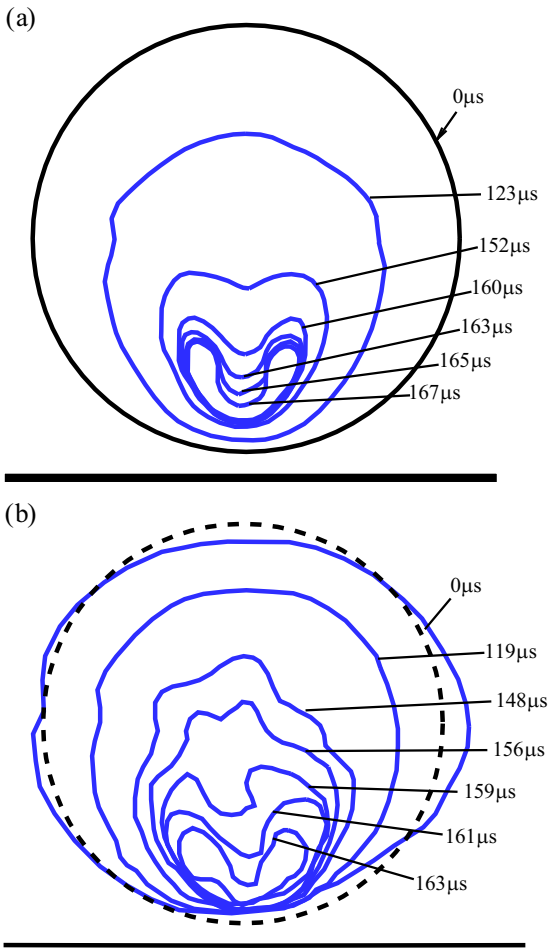

FIG. 1. Outlines of the cavitation bubble at various stages of collapse for (a) the present simulations and (b) experimental results from Kling and Hammitt [46].

neglect the second-order term in the origin formula, then a simple expression is obtained as

$$\kappa = 1 + 0.41 \frac{1}{2\gamma}. \tag{9}$$

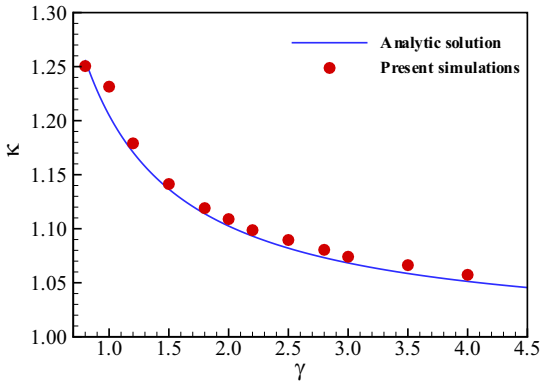

FIG. 2. Relationships between the dimensionless bubble-wall distance and the time span of bubble collapse. Solid line: the analytic solution from formula (9). Symbols: the present numerical simulations.

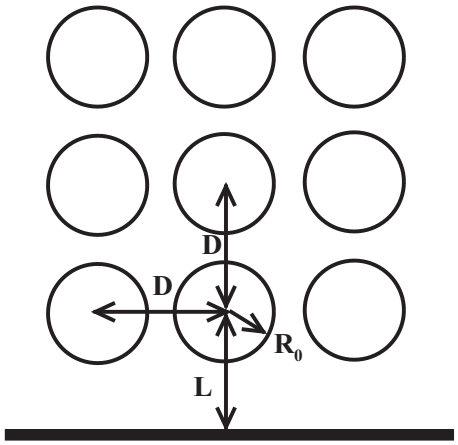

FIG. 3. Schematic of the geometric configuration for the simulations of 27 cavitation bubbles (side view).

Figure 2 clearly suggests that the time span is extended as the bubble is closer to the solid wall, indicating the constricting effect of the wall.

III. RESULTS

From the validation case in the last section, we understand that the asymmetry of bubble collapse can be brought by placing a solid wall, forming a jetting flow toward the wall. It can also be caused by the presence of nearby bubbles. In this section, we study the collapses of a cluster of cavitation bubbles, or more specifically, 27 bubbles, which are placed in a cubic region with three layers, and nine bubbles on each layer.

The initial configuration of the bubbles is shown in Fig. 3. All bubbles are initialized with the radius $R_0 = 1$ mm. The spacing between two adjacent bubbles is fixed at $D = 2.4$ mm, or a dimensionless value of $D^* = D/R_0 = 2.4$ for most cases. The ambient liquid pressure is set to 101 325 Pa, and the pressure inside the bubbles is 3169 Pa, therefore, the time span of collapse for an unbounded bubble with $R_0 = 1$ mm under these settings is $t_c = 92.3$ μs.

In Fig. 4, we present the evolutions of the vapor volumes and the wall center pressures as the bubbles collapse. The distances, ranging from $\gamma = 1.0$ to 3.5, are considered. In Fig. 4, the vapor volumes are scaled by the initial total volume of the 27 bubbles. We observe that the bubble cluster with a smaller distance from the wall collapses more slowly than the large distance clusters, indicating the constricting effect caused by the solid wall, which is consistent with the single bubble cases. We also observe that the time span for a bubble cluster is longer than that of a single bubble, by comparing Fig. 4(a) with Fig. 2. This further delay is caused by the nearby bubbles. Therefore, for multiple bubbles, the constrictions from both the solid wall and the nearly bubbles play roles on the process of collapse.

As we have learned from the previous experiments or our numerical simulations on a single bubble, as shown in Fig. 1(b), when the bubble collapses, intensive impulsive pressure can be induced on the wall due to the jetting flows caused by the nonspherical deformation of the bubble. When considering compressibility of the liquid, pressure waves can

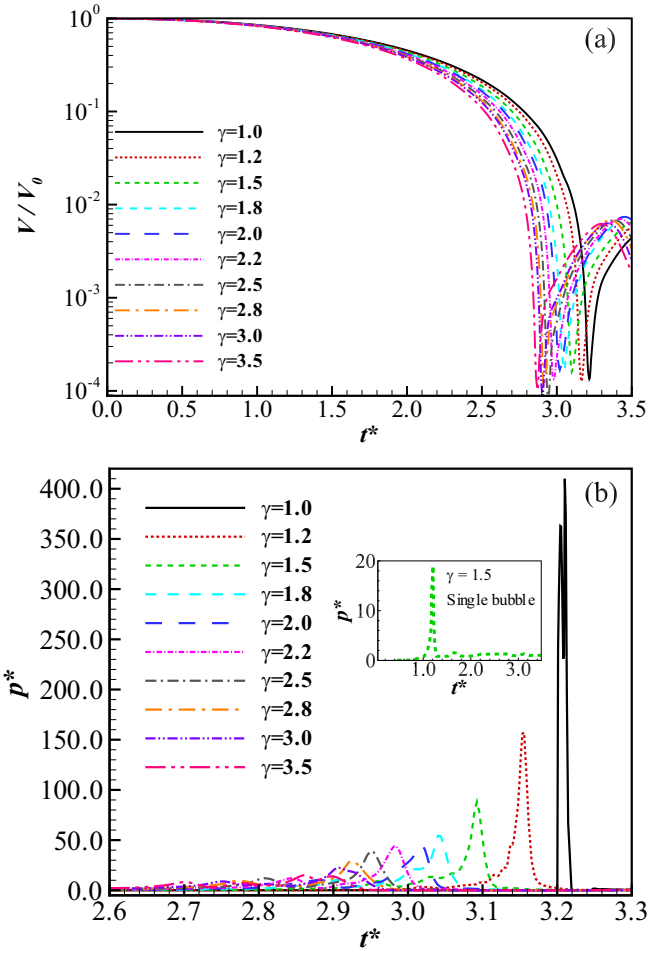

FIG. 4. Evolutions of (a) the vapour volumes and (b) the pressures at the center of the solid wall as the bubble cluster collapses, for different distances. The inset in (b) presents the pressure evolution at $\gamma = 1.5$ for a single bubble.

also be emitted as the bubble collapses to a minimum volume, or ideally a singular point, and these waves will eventually reach the solid wall. It is meaningful to examine the pressure variations on the wall, which are shown in Fig. 4(b). Here, the measuring point is located at the center of the solid wall, which is just underneath the central bubble on the lowest layer, as shown in Fig. 3. The peak value of the impulsive pressure on the wall increases as the distance is reduced, reaching up to a dimensionless pressure of 410 at $\gamma = 1.0$, or an absolute pressure of 41 MPa. To make a comparison with a single bubble, we show in the inset of Fig. 4(b) the pressure evolution for the single bubble at $\gamma = 1.5$, with a peak pressure of 20 observed. It shows that the impulsive pressure for a bubble cluster is nearly four times the single bubble case at the same distance from the wall. For example, the impulsive pressure reaches a peak about 100, or 10 MPa in absolute value, for a single bubble at $\gamma = 1.0$. This significant difference in impulsive pressure between single bubble and a bubble cluster indicates an apparent focusing of kinetic energy and pressure associated with the inward progress of collapse.

We understand that it is very difficult to make direction comparisons between numerical simulations and experiments

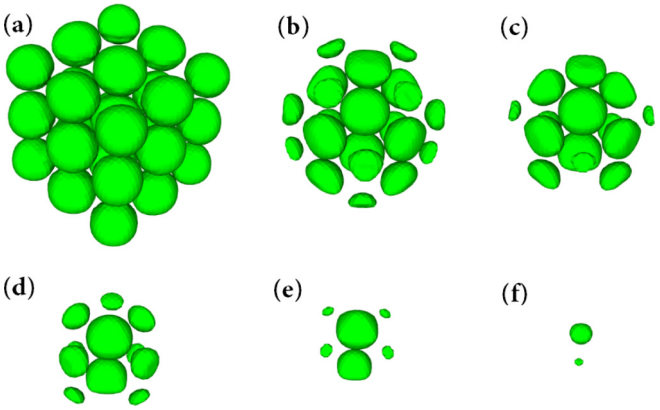

FIG. 5. Evolutions of the bubble shapes for $\gamma = 3.5$ at a sequence of time instants of (a) $t = 108$ μs, (b) $t = 202$ μs, (c) $t = 218$ μs, (d) $t = 234$ μs, (e) $t = 246$ μs, and (f) $t = 258$ μs.

on the impulsive pressures, due to the different pressure measuring facilities and different levels of accuracy of the sensors in the experiments. Yukio *et al.* [48] attached a pressure transducer to the wall covering an area with a diameter of 2.3 mm, which was larger than the induced bubbles, i.e., 1.0 and 1.7 mm considered in their experiments. Nevertheless, our simulated peak values of the impulsive pressure coincidentally fall into the range of their experiments, which is from 5 to 15 MPa. However, we should point out that the peak value of the pressure impulse is very sensitive to the spatial resolution in numerical simulations because the cavitation bubble collapses eventually to an infinitely small point, which causes singularity.

To get an intuitive understanding of the detailed dynamics during collapse, in Fig. 5, we present the instantaneous bubble shapes at a sequence of time instants for $\gamma = 3.5$. We note that these time instants correspond to the dimensionless times of $t^* = 1.17$, 2.19, 2.36, 2.54, 2.67, and 2.80, respectively. The last time instant is just before the vanishing of all bubbles, referring to Fig. 4. The nonsynchronous collapse is apparently observed among individual bubbles. As seen in Fig. 5(b), the outermost bubbles are the first to be exposed to the higher ambient pressure, thus the earliest to collapse, and the centermost bubble is the last to collapse, as seen in Fig. 5(f). This inward progress of collapse results in focusing of kinetic energy and pressure to centermost bubble, which has been quantitatively exhibited in Fig. 4.

It has been debated for many years whether cavitation damage is caused by microjets or by shock waves or by both [4]. In other words, which mechanism is the major contribution to the intensive impulsive pressure on the wall, as we have discussed for Fig. 4. Kimoto [49] declared that the impulsive pressures from the collapse shock were two to three times larger than those due to the microjets, though both may contribute to the impulsive loading of the surface. However, we note that the shock was actually induced by a remnant cloud of small bubbles that continued to collapse collectively after collapse of a single bubble in their experiments [49].

In Fig. 6, we present the velocity vectors projected onto the symmetry plane at different time instants for $\gamma = 3.5$, corresponding to Figs. 5(c)–5(f). The inward progress of collapse

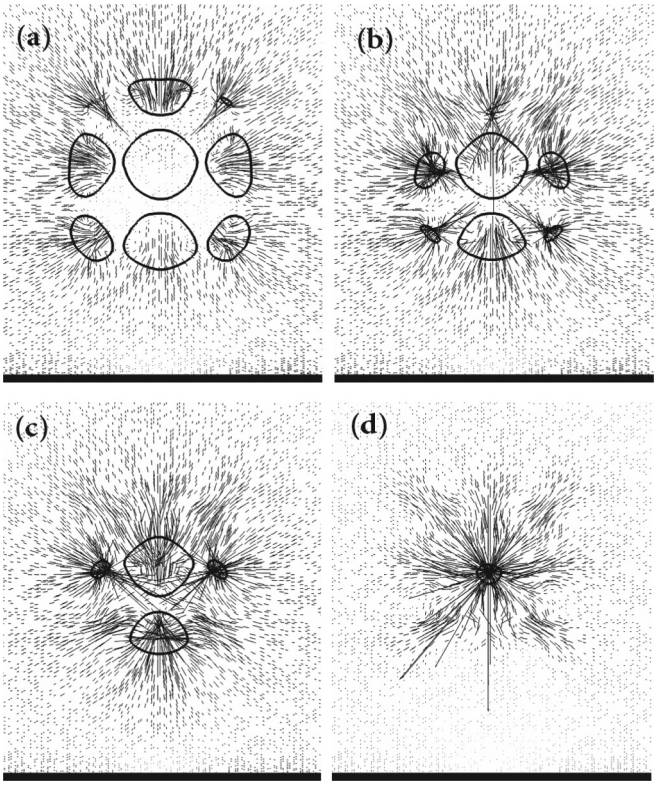

FIG. 6. Velocity vectors within the symmetry plane for $\gamma = 3.5$ at different time instants of (a) $t = 218$ μs, (b) $t = 234$ μs, (c) $t = 246$ μs, and (d) $t = 258$ μs.

is exhibited more clearly in this figure. The asymmetrical dynamics of the bubbles surrounding the central one, particularly the reentrant jetting is clearly observed. For example, if we examine the uppermost bubble in Fig. 6(a), we can see that the nonspherical deformation causes the upper side of the bubble to accelerate inward more rapidly than the opposite side and this results in the development of a high-speed reentrant microjet which penetrates the bubble. As seen in Fig. 6(d), at the late stage of collapse, since the centermost bubble is the last to collapse, it actually determines the details of this jetting and the actual potential for wall damage. However, since the microjet's function within a very local region (apparently shown in Fig. 6), their damages to the wall would be very limited, particularly in the cases when the bubble or the bubble cluster is a certain distance away from the wall. That is why

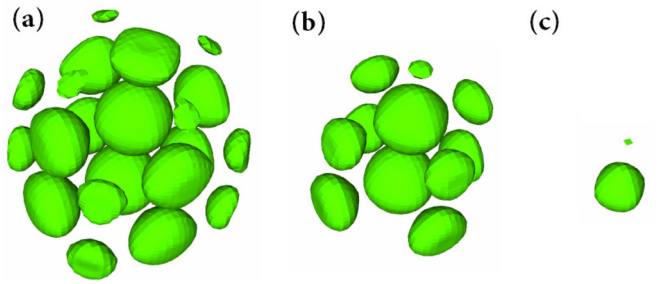

FIG. 7. Evolutions of the bubble shapes for $\gamma = 1.5$ at different time instants of (a) $t = 214$ μs or $t^* = 2.32$, (b) $t = 240$ μs or $t^* = 2.60$, and (c) $t = 274$ μs or $t^* = 2.97$.

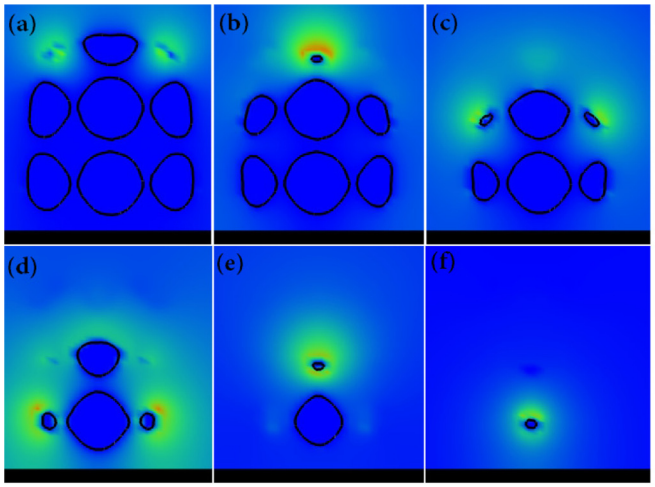

FIG. 8. Pressure contours within the symmetry plane for $\gamma = 1.5$ at different time instants of (a) $t = 220$ μs, (b) $t = 242$ μs, (c) $t = 256$ μs, (d) $t = 266$ μs, (e) $t = 274$ μs, and (f) $t = 282$ μs. Blue (dark gray) and red (light gray) colors denote low and high values of pressure, respectively.

we can only identify a single primary peak in the pressure impulse shown in Fig. 4(b). Another possible explanation is that because the pressure wave propagates at a very high speed, thus reaching the wall earlier than the jetting flows, it is nearly impossible to distinguish the contribution from that induced by the pressure waves.

As the bubble cluster is closer to the wall, as shown in Fig. 7 for $\gamma = 1.5$, a markedly different sequence of collapse is observed, in contrast to Fig. 5 for $\gamma = 3.5$. Here, the central bubble nearest to the wall is the last to collapse, as seen in Fig. 7(c). This sequential collapse can also been identified from the pressure fields, as shown in Fig. 8. We note that high pressure generates as an individual bubble nearly vanishes.

To investigate the pressure propagation in space, in Fig. 9, we present the radial distributions of pressure on the wall along the symmetry line crossing the measuring point used for Fig. 4. It is clearly seen that the peak value decreases as the pressure wave travels away from the central point, behaving as a typical characteristic of spherical waves. It is straightforward to estimate the speed of wave propagation, for example, in a simple manner, by measuring the distance

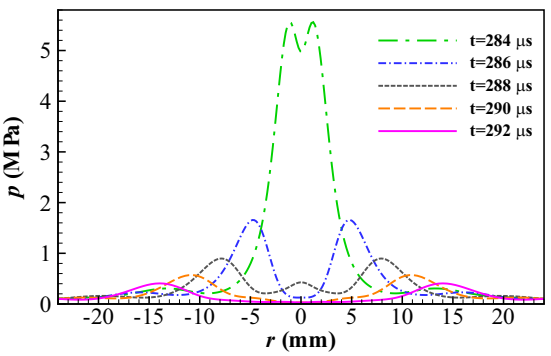

FIG. 9. Radial distributions of the pressure on the wall for a sequence of time instants ($\gamma = 1.5$).

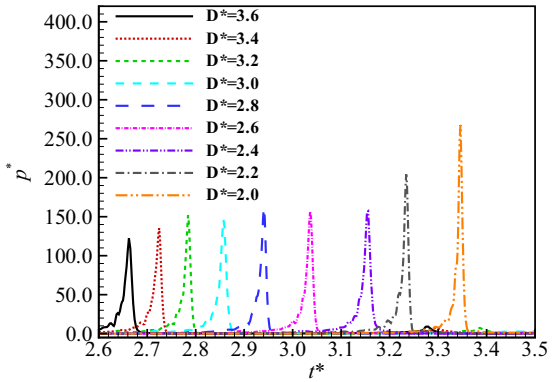

FIG. 10. Evolutions of the pressures at the center of the solid wall as the bubbles collapse for different bubble-bubble spacings with a fixed bubble-wall distance of $\gamma = 1.2$.

between two adjacent peaks from Fig. 9. As the wave travels from $r = 1.299$ mm at 284 μs to $r = 14.053$ mm at 292 μs, resulting in a traveling speed of 1594 m/s, around the speed of sound used in Eq. (6).

Moreover, we also investigate the variations of impulsive pressure with the bubble-bubble spacing. As shown in Fig. 10, at a fixed bubble-wall distance $\gamma = 1.2$, the peak pressure does not change much as the bubble-bubble spacing is reduced from $D^* = 3.6$ to 2.4, until the bubbles are very closely deployed, e.g., $D^* = 2.2$ and 2.0. We note that the bubbles are actually attached to their adjacent bubbles for $D^* = 2.0$, according to the definition in Fig. 3. It also suggests that the constricting effect brought by the nearby bubbles is not as significant as that brought by the solid wall.

IV. CONCLUSIONS

In this paper, direct numerical simulations (DNS) have been performed to study the collapse of multiple cavitation bubbles or a bubble cluster, with 27 bubbles considered. A transport equation for the liquid volume fraction is adopted to resolve the interface between two phases. It is assumed that the bubbles are filled with vapor with constant density and pressure, while the liquid outside of the bubbles is compressible and its compressibility is represented by a state equation. This simplified numerical model has been proved to be feasible and efficient to the study of bubble collapse, particularly when there are multiple bubbles grouped into a cluster.

In our simulations, we concentrate on the peak value of the pressure impulse imposed on the constricting wall. As we have discussed, this impulsive pressure is induced, for the greater part, by the pressure wave emitted from the bubble collapse. The impulsive pressure varies with the bubble-wall distance and bubble-bubble spacing, in which the bubble-wall distance plays the most significant role. At a fixed bubble-bubble spacing $D^* = 2.4$, a maximum pressure of 41 MPa is found when the bubble cluster is very close to the wall, which is consistent with the previous experiments, at least in the same order of magnitude. We have pointed out that a direct comparison with experiments in the absolute value of impulsive pressure is very difficult since the bubble collapses

eventually to a minimum cavity volume, or ideally a singular point, which requires an extremely fine spatial resolution in the numerical model.

By examining the evolutions of bubble shapes and flow fields, the inward progress of collapse is clearly exhibited, and we identify two distinctly different sequences of collapse between small and large bubble-wall distances, demonstrating a significant constricting effect from the wall. At a large bubble distance, the centermost bubble of the cluster is the last to collapse, while at a small bubble distance, it is the central bubble nearest to the wall which collapses lastly. This difference can also explain the more intensive impulsive pressure for the smaller bubble-wall distances.

We have provided a numerical approach to investigate the collapse of a bubble cluster, presenting the detailed evolutions of bubble shapes and flow fields, and the impulsive pressure on the wall has been evaluated. The underlying physical mechanism of bubble collapse is still poorly understood, which is worth further investigations. More factors should be considered in future studies, for example, phase transition and detailed resolution of flow inside the bubble.

ACKNOWLEDGMENTS

This research has been supported by the National Natural Science Foundation of China (Grant No. 11772298) and the State Key Program of National Natural Science of China (Grant No. 91852204).

[1] L. Shengcai, *Cavitation of Hydraulic Machinery* (World Scientific, Singapore, 2000), Vol. 1.
[2] W. Lauterborn and H. Bolle, J. Fluid Mech. **72**, 391 (1975).
[3] J. Dear and J. Field, J. Fluid Mech. **190**, 409 (1988).
[4] C. E. Brennen, *Cavitation and Bubble Dynamics* (Cambridge University Press, Cambridge, UK, 2014).
[5] K. S. Suslick, Science **247**, 1439 (1990).
[6] S. Hilgenfeldt, S. Grossmann, and D. Lohse, Nature (London) **398**, 402 (1999).
[7] P. Marmottant and S. Hilgenfeldt, Nature (London) **423**, 153 (2003).
[8] C. E. Brennen, Interface Focus **5**, 20150022 (2015).
[9] M. P. Stewart, A. Sharei, X. Ding, G. Sahay, R. Langer, and K. F. Jensen, Nature (London) **538**, 183 (2016).
[10] Y. Wang and D. S. Kohane, Nat. Rev. Mater. **2**, 17020 (2017).
[11] L. Rayleigh, Philos. Mag. **34**, 94 (1917).
[12] M. S. Plesset, J. Appl. Mech. **16**, 277 (1949).
[13] B. E. Noltingk and E. A. Neppiras, Proc. Phys. Soc., Sect. B **63**, 674 (1950).
[14] H. Portisky, in *Proceedings of the First US National Congress on Applied Mechanics* (ASME, New York, 1952), pp. 813–821.
[15] J. Keller, J. Acoust. Soc. Am. **68**, 628 (1980).
[16] D. Fuster and T. Colonius, J. Fluid Mech. **688**, 352 (2011).
[17] O. Vincent, P. Marmottant, P. A. Quinto-Su, and C.-D. Ohl, Phys. Rev. Lett. **108**, 184502 (2012).
[18] O. Vincent and P. Marmottant, J. Fluid Mech. **827**, 194 (2017).
[19] Q. Wang, Phys. Fluids **29**, 072101 (2017).
[20] A. A. Doinikov, B. Dollet, and P. Marmottant, Phys. Rev. E **97**, 013108 (2018).
[21] M. Kornfeld and L. Suvorov, J. Appl. Phys. **15**, 495 (1944).
[22] M. S. Plesset and R. B. Chapman, J. Fluid Mech. **47**, 283 (1971).
[23] A. Vogel and W. Lauterborn, J. Acoust. Soc. Am. **84**, 719 (1988).
[24] A. Vogel and W. Lauterborn, Appl. Opt. **27**, 1869 (1988).
[25] Y. Tomita, A. Shima, and K. Sato, Appl. Phys. Lett. **57**, 234 (1990).
[26] B. Han, K. Köhler, K. Jungnickel, R. Mettin, W. Lauterborn, and A. Vogel, J. Fluid Mech. **771**, 706 (2015).
[27] L. W. Chew, E. Klaseboer, S.-W. Ohl, and B. C. Khoo, Phys. Rev. E **84**, 066307 (2011).
[28] Y. Tomita and K. Sato, J. Fluid Mech. **819**, 465 (2017).
[29] S. Li, A. Zhang, R. Han, and Y. Liu, Phys. Fluids **29**, 092102 (2017).
[30] E.-A. Brujan, T. Noda, A. Ishigami, T. Ogasawara, and H. Takahira, J. Fluid Mech. **841**, 28 (2018).
[31] J. R. Sukovich, P. A. Anderson, A. Sampathkumar, D. F. Gaitan, Y. A. Pishchalnikov, and R. G. Holt, Phys. Rev. E **95**, 043101 (2017).
[32] M. Ida, T. Naoe, and M. Futakawa, Phys. Rev. E **75**, 046304 (2007).
[33] K. Y. Lim, P. A. Quinto-Su, E. Klaseboer, B. C. Khoo, V. Venugopalan, and C.-D. Ohl, Phys. Rev. E **81**, 016308 (2010).
[34] P. Cui, Q. Wang, S. Wang, and A. Zhang, Phys. Fluids **28**, 012103 (2016).
[35] D. Veysset, U. Gutiérrez-Hernández, L. Dresselhaus-Cooper, F. De Colle, S. Kooi, K. A. Nelson, P. A. Quinto-Su, and T. Pezeril, Phys. Rev. E **97**, 053112 (2018).
[36] N. Bremond, M. Arora, C.-D. Ohl, and D. Lohse, Phys. Rev. Lett. **96**, 224501 (2006).
[37] I. van der Kroon, P. A. Quinto-Su, F. Li, and C.-D. Ohl, Phys. Rev. E **82**, 066311 (2010).
[38] G. L. Chahine, *Bubble Dynamics and Interface Phenomena* (Springer, Berlin, 1994), pp. 195–206.
[39] T. T. Bui, E. T. Ong, B. C. Khoo, E. Klaseboer, and K. C. Hung, J. Comput. Phys. **216**, 430 (2006).
[40] J. Zhang, L. Zhang, and J. Deng, Water **11**, 247 (2019).
[41] J. Huang and H. Zhang, Acta Mech. Sin. **23**, 645 (2007).
[42] E. Can and A. Prosperetti, J. Comput. Phys. **231**, 1533 (2012).
[43] A. Tiwari, C. Pantano, and J. Freund, J. Fluid Mech. **775**, 1 (2015).
[44] H.-T. Chen and R. Collins, J. Comput. Phys. **7**, 89 (1971).
[45] L. Zhang and B. C. Khoo, Ocean Eng. **87**, 174 (2014).
[46] C. L. Kling and F. G. Hammitt, J. Basic Eng. **94**, 825 (1972).
[47] M. Rattray, Perturbation effects in cavitation bubble dynamics, Ph.D. thesis, California Institute of Technology, 1951.
[48] Y. Tomita, A. Shima, and T. Ohno, J. Appl. Phys. **56**, 125 (1984).
[49] H. Kimoto, *International ASME Symposium on Cavitation Research Facilities and Techniques* (ASME, New York, 1987), pp. 217–224.